

Single and Coupled EOF Analysis of GRACE-Follow-On and ICESat-2 Data

Abinay Brown and Andrew Wood

Georgia Institute of Technology, Atlanta, Georgia, 30332

Overlapping observations from the Gravity Recovery and Climate Experiment Follow-On (GRACE-FO) and Ice, Cloud, and Land Elevation Satellite-2 (ICESat-2) were examined to study variation in ice mass and elevation over the duration of 2019-2021. To visualize the temporal and spatial components of these variations, time series from each satellite data product were approximated using empirical orthogonal functions (EOFs). The data was reconstructed using the first three primary EOF modes and expansion coefficients, which corresponded to the dominant change signals in the region. For the GRACE-FO data, these modes were found to explain approximately 87% of the variance. For ICESat-2, 90.4% of the variance could be described by the first two modes. To compare the patterns of variation for the two datasets, singular value decomposition (SVD) was performed for the coupled fields. The results of this analysis found that the first mode was responsible for over 99% of the variance between the two fields. The strong correlation between the datasets indicates a common general trend, though further filtering may provide further insight into shared sub-annual signals.

I. Nomenclature

A	= column vector of percent variance explained by respective modes
E	= matrix of expansion coefficients
N^t	= transpose of a matrix
S	= matrix of eigenvectors of UU^t
U	= data matrix
V	= matrix of eigenvectors of covariance matrix
Λ	= diagonal matrix of squared eigenvalues
λ	= column vector of diagonal elements of Λ

II. Introduction

Recent study of the Antarctic region has shown significant rates of mass and volume decrease. In this study, variable gravity data from Gravity Recovery and Climate Experiment Follow-On (GRACE-FO) and ice elevation data from Ice, Cloud, and Land Elevation Satellite-2 (ICESat-2) were analyzed to provide insight into the trends, annual variations, and sub-annual variations that compose these changes to the ice sheet.

GRACE-FO, a follow up to the original GRACE satellite pair that recorded variable gravity data from 2002 to 2017, was launched in May of 2018 and began collecting data one month later. Derived from sensor measurements from a comparison of onboard accelerometers and GPS receivers, GRACE Level-2 datasets consist of spherical harmonic coefficients for the variable gravity field. The Level-3 products, used for this report, contain several layers of pre-processing and are produced as one-degree grids.

For this research study, the data from the ICESat-2 satellite part of the NASA's Earth Observing System and a successor of the ICESat-1 mission, is used for analyzing ice-levels. The ICESat-2 is equipped with Advanced Topographic Laser Altimetry system (ATLAS) LIDAR that measures the travel of 532nm wavelength laser photons reflected from the surface of the Earth. The LIDAR system has an array of 6 beams rotated 2 degrees outwards such that it covers 3.3km across track and 2.5km along track. The laser operates at 10kHz sending trillions of photons some of which are reflected back onto a beryllium telescope.

In this report, we will use Level-3A ATL06 land-ice data [1], which are geolocated photon data recorded from Antarctica during the years 2019-2021 to find the seasonal rates of Land-ice change levels, perform power spectrum analysis for key locations on the West coast, EOF analysis for spatial and temporal variations of land-ice level change, and EOF coupled Icesat-2 and Grace covariance analysis.

III. Methodology

A. GRACE-FO Analysis

1. Data

This study contains an analysis of the empirical orthogonal functions that describe spatial and temporal trends between elevation and ice mass changes in the Antarctic region. The datasets used for this project are Level-3 GRACE Follow-On products from the Center for Space Research at the University of Texas at Austin (CSR) [1]. This set was derived from the Level-2 monthly spherical harmonic coefficient output. Reprocessing for the Level-3 data includes geocenter, glacial isostatic adjustment (GIA), C_{20} coefficient, and C_{30} coefficient corrections, as well as Gaussian smoothing. A diagram explaining the process can be seen in Figure 1.

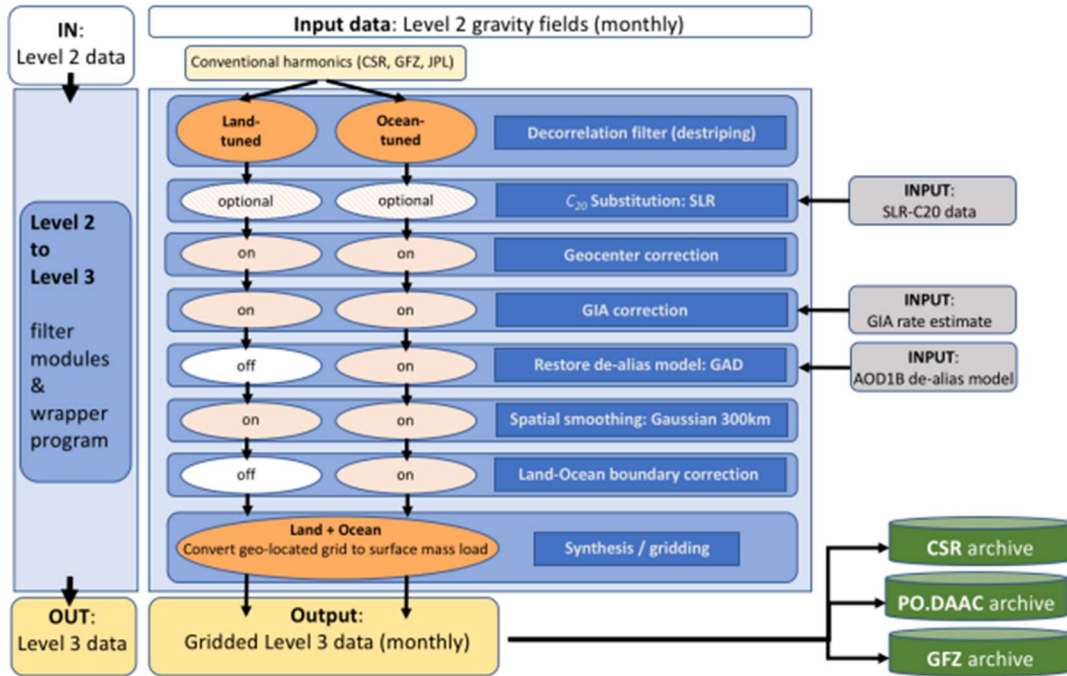


Figure 1 GRACE Level-3 Processing Flowchart

Each set contains one-degree gridded data of mass anomalies over the land in a specified period, and is measured in equivalent water height, used interchangeably with equivalent water thickness. Further information can be found in the GRACE L-3 Product User Handbook [2]. Because the primary focus of this analysis was to compare mass and elevation changes over the region of interest during the overlapping period of GRACE-FO and ICESat-2, only grids inside the interval from January 2019 to December 2021 were utilized.

2. Time Series and Spectral Analysis

In order to properly understand dominant trends in mass variation identified by more complicated forms of analysis, fixed grid points were studied with time series and spectral analysis. Each monthly gridded dataset was modified to reflect a basic cumulative sum, using the January 2019 set as a baseline. The equivalent water height values of all previous datasets were added to datasets after that time period, so that each would represent a total

mass change from the reference date, as opposed to a monthly mass rate. Figures were then plotted for each timestep. The 104.5° W line of longitude was selected for further study because of the variation of trend along the line. Time series were plotted for 87.5° (A), 81.5° (B), and 77.5° (C) S, which can be seen in Figures 3-5. Figure 2 below highlights these points geographically.

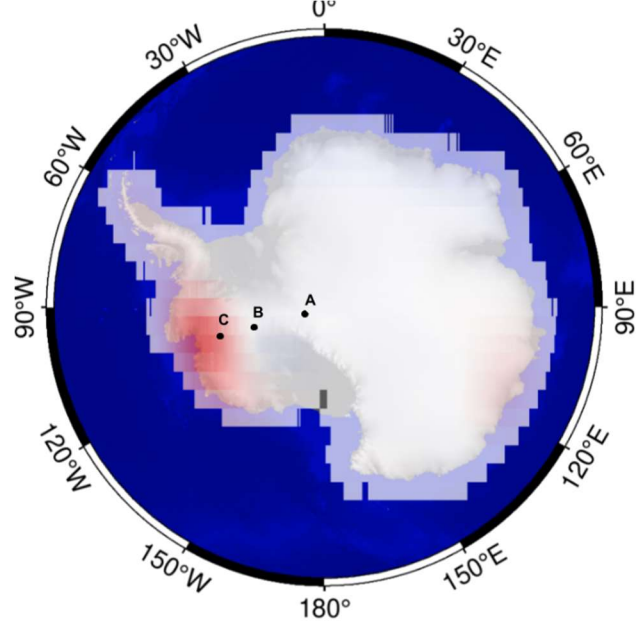


Figure 2 GRACE Level-3 Processing Flowchart

Because of gaps within the full time series of GRACE and GRACE-FO data output, a Lomb-Scargle least squares spectral analysis method was used to determine the frequency of sinusoidal trends present within the time series. This method utilizes a standard discrete Fourier transform for uniform intervals in the data, and calculates power based on the amplitude of sine and cosine components of the generalized form, determined with a least squares best fit method [3].

3. EOF Analysis

The empirical orthogonal function method, or EOF, is a method of finding both time and spatial patterns (EOFs), and the corresponding time series (as expansion coefficients) for a dataset that varies in both time and space. It is frequently used in climate studies to determine spatial and temporal modes of variability [4].

To perform this, the time series for each grid point was arranged into a data matrix U , where each column corresponds to a grid center described by a longitude and latitude value and each row to a timestep within the time series. For a traditional EOF analysis, a couple of steps would be required. After the means of each set of observations was removed, the covariance matrix $U^t U$ would be found. The EOF modes would be found by finding the eigenvalues and eigenvectors of this matrix. The largest eigenvalues and corresponding eigenvectors would indicate the most prevalent modes, and the percent variance explained by each would be determined. Expansion coefficients could be determined by projecting the data matrix U onto each EOF.

As described by Björnsson and Venegas [6], though, this process can also be performed using singular value decomposition (SVD) for a set of observations stored in U . Each row was then detrended using a linear regression fit to remove the mean and overarching trend in attempt to isolate the annual and sub-annual signals. U was then decomposed according to Equation 1:

$$SAV = \text{SVD}(U) \quad (1)$$

So that:

$$S\Lambda V^t = U \quad (2)$$

The column vectors of V hold the eigenvectors of the covariance matrix for U , the diagonal of Λ holds the squared eigenvalues, and the columns of S contain the eigenvectors for UU^t , or the normalized time series. The expansion coefficients, stored in the matrix E , were then calculated by multiplying the S matrix by the diagonal matrix Λ , as shown in Equation 3:

$$E = SA \quad (3)$$

The matrix of expansion coefficients E was calculated to contain one row for each timestep in the time series and one column for each mode, equal to the number of grid points. The time series of these coefficients for the three most influential modes, with percent variance explained as calculated below, can be seen in Figures 6-8. As previously done with the general time series for the data, Lomb-Scargle periodograms were produced to examine the temporal frequency components of the expansion coefficient time series for the first three modes, which can be seen in the same Figures.

Alongside this, the percent variance on each EOF mode was determined using Equation 4, where λ represents a column vector with each diagonal value of Λ . \circ describes an elementwise multiplication.

$$A = \frac{\lambda \circ \lambda}{\text{trace}(\Lambda)} \quad (4)$$

The resulting column vector A holds the percent variance explained by the first mode in the first row, the second mode in the second row, and so on. The first three modes were found to be responsible for 87% of the overall variance in the data, and these were selected for further study.

Finally, a reconstruction of the data with only the three principal modes was determined with Equation 5, where the asterisk represents an entire row or column.

$$U_{\text{reconstruct}} = \sum_{j=1}^{n=3} E_{*,j} * V_{j,*}^t \quad (5)$$

Individual plots of the spatial footprint of the three selected modes at the first and second timesteps may be seen in Figures 9-12.

B. ICESAT Analysis

1. Data Acquisition and Averaging

For this research, level-3A Geolocated Photon Land-Ice data is acquired from NSIDC organized by months and Coasts starting 2019 to 2021 for a total of 36 months. The requested data contains altitude points from all 6 laser beams to maximize coverage. The location analyzed spans from latitudes 61.5° S to 90°S and longitudes -180°W and 180°E. The data is download using the Icexpy API for python [8].

The geolocated photon altitude data was recursively averaged into 0.5°x0.5° grids and 1°x1° grids. The half degree grids were used for majority of analysis and the 1-degree grids were used for combined Icesat and Grace data correlation analysis; the 1-degree sizing was due to the resolution of the Grace level-3 data. For averaging, the data was down sampled to 2000Hz; the ATLAS system samples at 10kHz, and every 5th measurement was

used. The half degree grids contained 41,040 grid locations, and the 1-degree grids had 10,080 grid locations, where the grid centers represent the averages.

Processing and sorting over billions of data points were done using the Georgia Tech PACE Cluster using multiple nodes and processors running programs in parallel. The sorting and averaging were done using multithreading to lower the total run time.

2. Land-Ice Change Rates

With the averaged land-ice level for 36 months for each of the grid cells, the time derivative is taken to give the Land-Ice change rates. In this report, we focus on the land-ice rates for March, June, September, and December from 2019 to 2021; during the Vernal Equinox, Summer Solstice, Autumnal Equinox, and Winter Solstice to understand evolution Ice-level changes over the years during the months of the season change.

3. Power Spectrum Analysis

With the monthly time series for the averaged gridded ice-levels, the power spectrum via Fast-Fourier-Transform is obtained to analysis periodic nature of ice-level changes over the years. Decomposing the signal into the frequency domain will allow us to determine the peak amplitudes and frequencies that accounts for the major ice-level change. Over the past few years, the Antarctica west coast has seen major changes in ice-levels, therefore, we will be looking at three locations 87.5°S 104.5°W, 81.5°S 104.5°W, and 77.5°S 104.5°W in particular. Similarly, the power spectrum of the Grace data for these key locations will determined to ascertain if the periodic nature of the Ice-level change gets reflected in the Grace gravimetry results indicating a correlation between the ice-mass change and the gravitational potential change.

4. Icesat-2 EOF Analysis

The Empirical Orthogonal Functions, EOF, is a method to decompose the time series of a given data quantity at several locations into Spatial and Temporal components [6]. This allows us to determine the primary modes, EOFs, that constitute the majority of the variance in the given data and the time series of these modes (corresponding Expansion Coefficients).

Singular Value Decomposition (SVD) is used on a matrix containing the monthly land-ice levels in rows, and the columns representing each grid location resulting in a 36x7681 matrix. The data is detrended by subtracted the initial Land-Ice level (Jan 2019) for each of the grid cells. The SVD then decomposes the matrix into the U, S, and V matrices, where the S matrix contains the modes/ square roots of the eigenvalues of the EOFs along the diagonals, the columns of the V matrix contain the eigenvectors or the EOFs.

To understand the variation of the modes over time, the expansion coefficients can be derived using equation 3, where the rows of the resulting matrix give the time series of the modes (given by the column). The EOFs are uncorrelated in Space whereas the expansion coefficients are uncorrelated in time. In this analysis, we pick the top 2 primary modes that account for majority of the variances in the data which is then normalized using equation 4. The top two modes are then used to reconstruct the original data using equation 5, this allows us to remove the variations due to noise.

5. Icesat-2 and Grace Coupled EOF Analysis

The same approach is used for the Icesat-2 and Grace Coupled EOF Analysis. In this case, the Covariance matrix of the two data sets is used. The individual data sets time series at different locations arranged in a similar manner as before, having dimensions, 36x7681 containing the land-ice levels and another matrix 36x7681 containing the Equivalent Water heights levels from Grace level-3 data. The covariance matrix is then found using equation 6, where X is the matrix for Icesat-2 data set, and Y matrix contains the Grace data set, both data sets are detrended by subtracting the averages of the individual time series of each of the locations before being plugged into the equation. N is the number of time samples, in this case it is 36, for the 36 months between 2019 and 2021.

$$\text{Covariance} = \frac{X^T Y}{N} \quad (6)$$

This results in a 7681x7681 covariance matrix on which SVD is performed to determine the U, S, and V matrices. The Singular Value Decomposition on this large covariance matrix is performed on Georgia Tech's PACE cluster which was executed on 4 nodes, having 2 processors each of 2GB memory, which was completed significantly faster than it would on a personal computer.

In this coupled EOF analysis, the S matrix contains the modes/square roots of the eigenvalues of the EOFs, equation (7) and (8) can be used to determine the expansion coefficients of the modes for the case of Icesat and Grace (The columns of the resulting matrix give the time series of the modes). This allows us to see the variations of the modes that affect the covariances of the Icesat and Grace data. We use equation 4 to determine the Squared-Covariance-Fractions/modes of the data set.

$$A = XU \quad (7)$$

$$B = YV \quad (8)$$

Similarly, we pick the top 2 modes that contribute to most of the variance in the covariance of the Icesat and Grace data and then reconstruct the original covariance matrix using the top 2 modes allowing us to filter for noise.

IV. Results

C. GRACE-FO Analysis

1. Time Series and Spectral Analysis

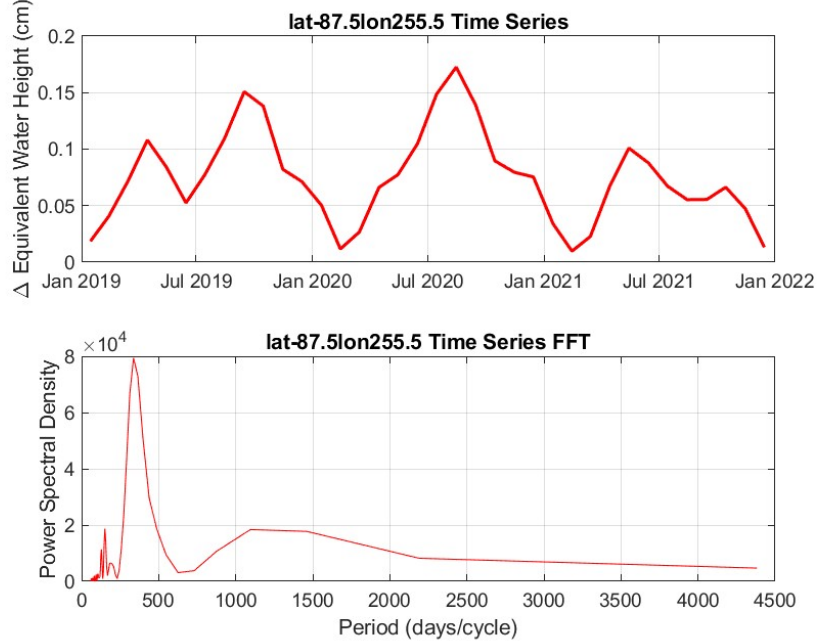


Figure 3 Time Series and Lomb-Scargle Periodogram for Point A (87.5° S, 104.5° W)

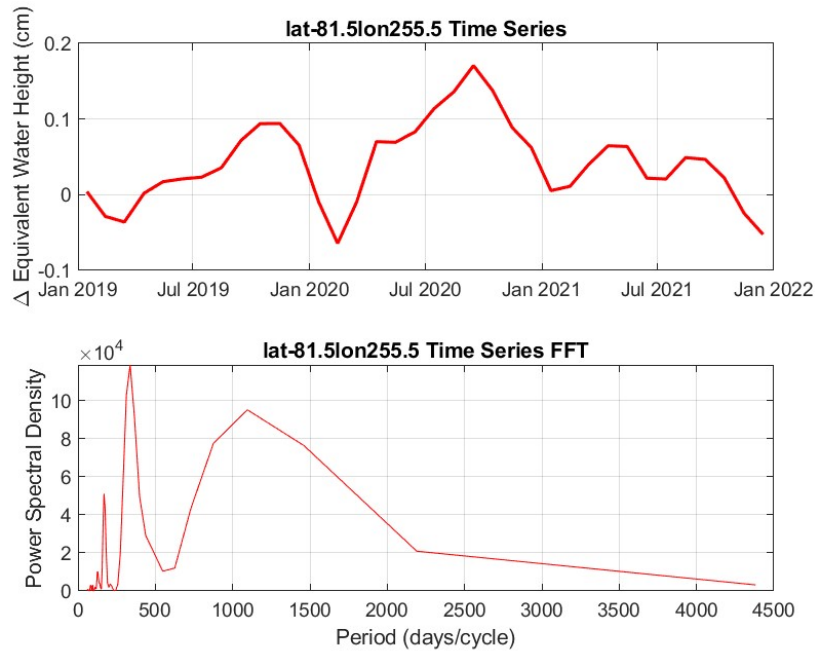


Figure 4 Time Series and Lomb-Scargle Periodogram for Point A (81.5° S, 104.5° W)

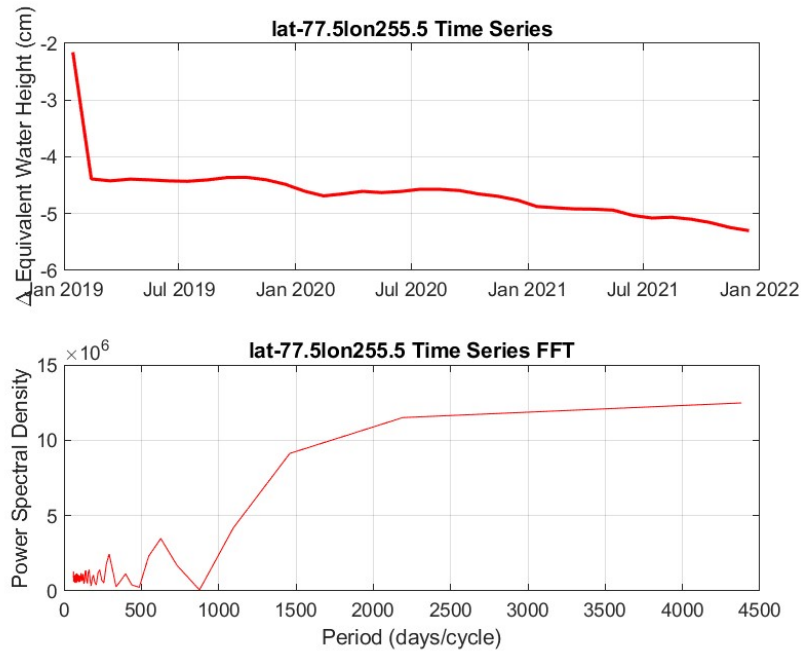


Figure 5 Time Series and Lomb-Scargle Periodogram for Point A (77.5° S, 104.5° W)

2. EOF Analysis

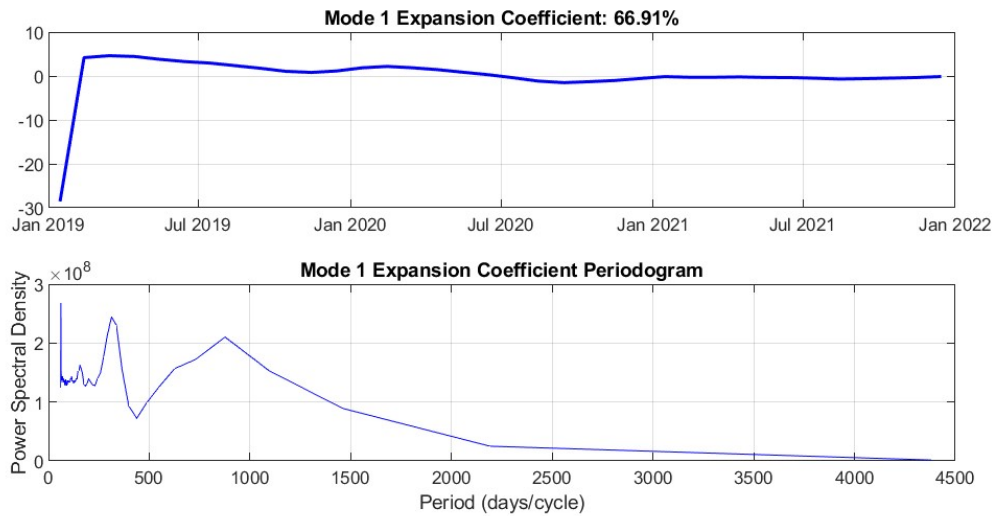


Figure 6 Time Series and Lomb-Scargle Periodogram of Expansion Coefficient for Mode 1

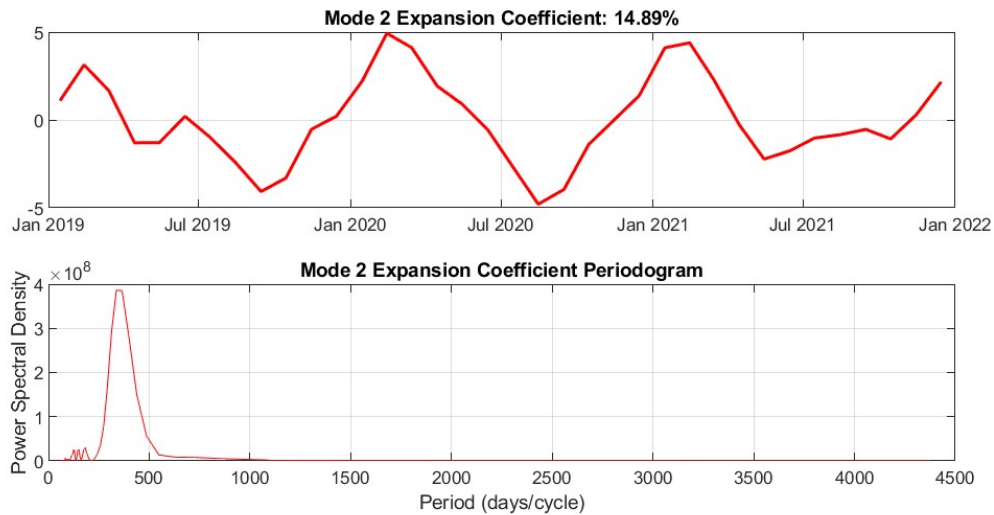


Figure 7 Time Series and Lomb-Scargle Periodogram of Expansion Coefficient for Mode 2

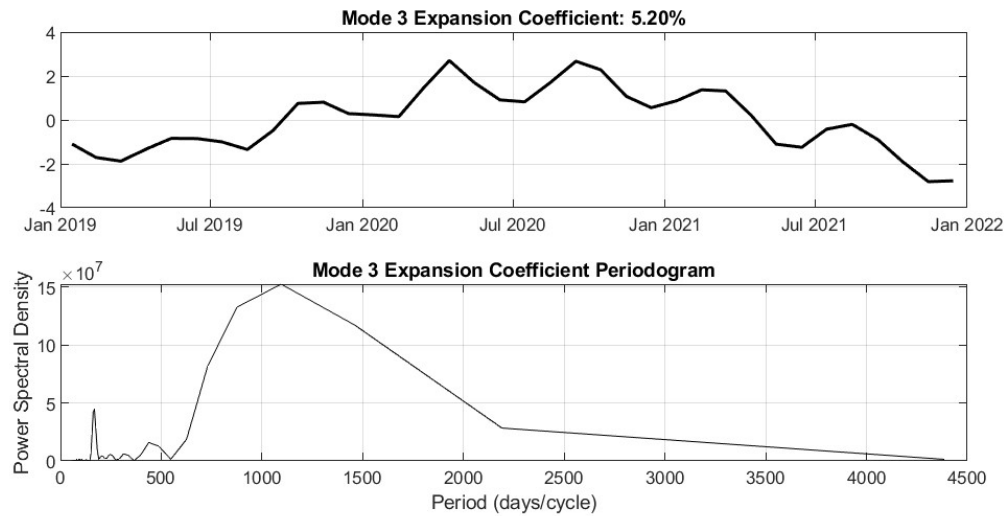


Figure 8 Time Series and Lomb-Scargle Periodogram of Expansion Coefficient for Mode 3

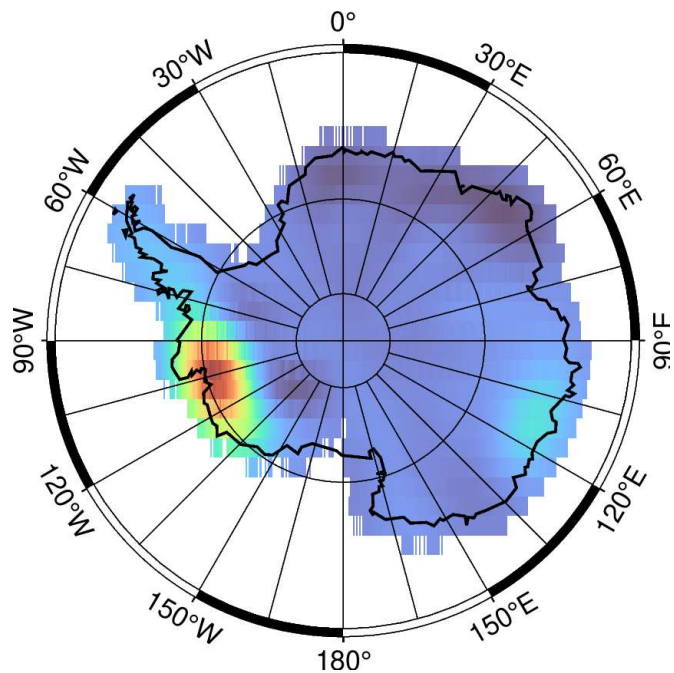


Figure 9 Timestep 1 of EOF Mode 1, Accounting for 66.91% of Variance

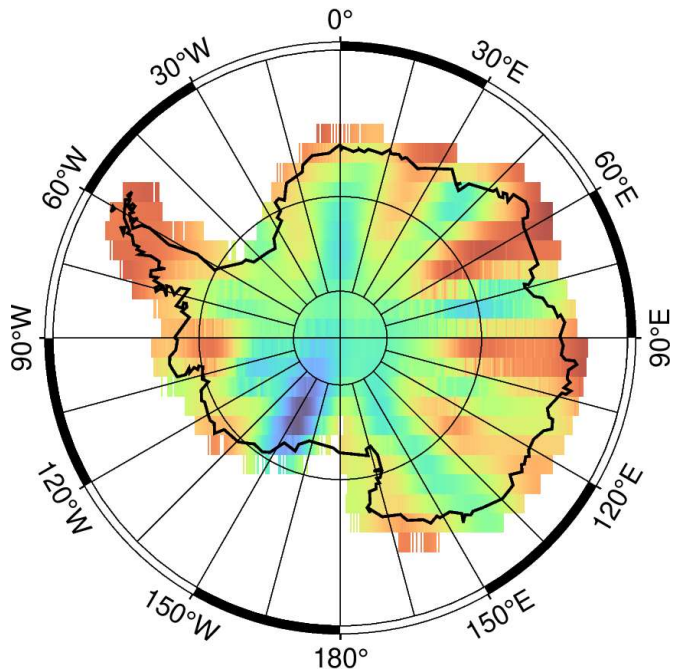


Figure 10 Timestep 1 of EOF Mode 2, Accounting for 14.89% of Variance

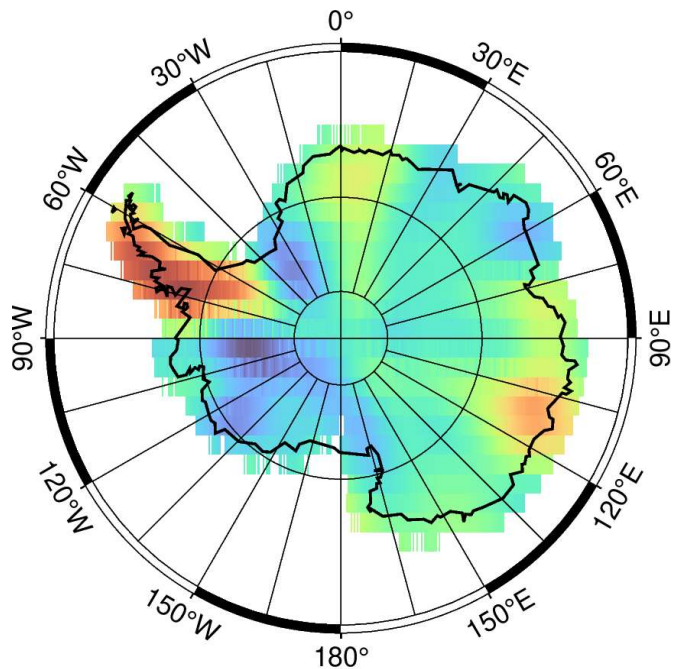


Figure 11 Timestep 1 of EOF Mode 3, Accounting for 5.20% of Variance

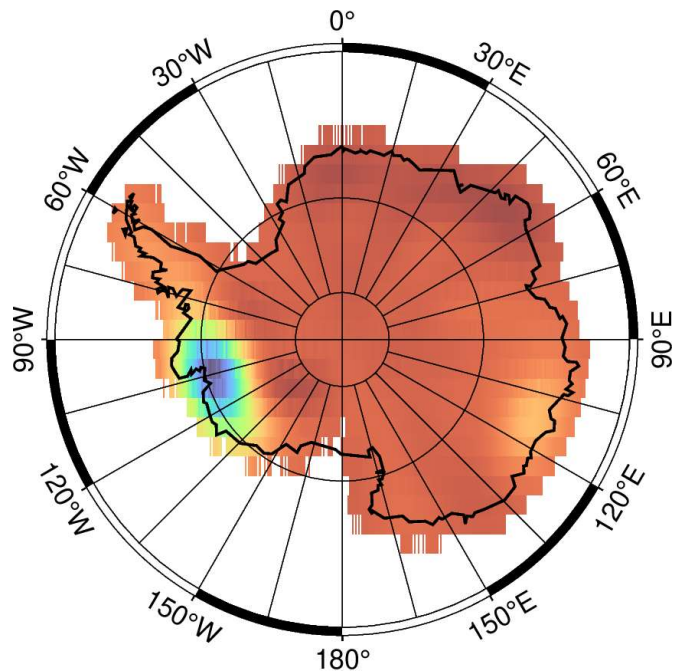


Figure 12 Timestep 2 of EOF Mode 1, Accounting for 66.91% of Variance

D. ICESAT Analysis

1. Vernal Equinox Land-Ice Change Rates

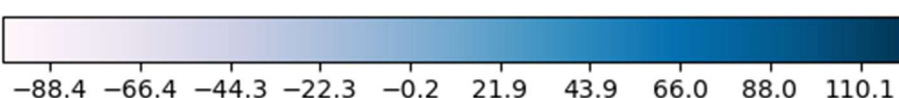
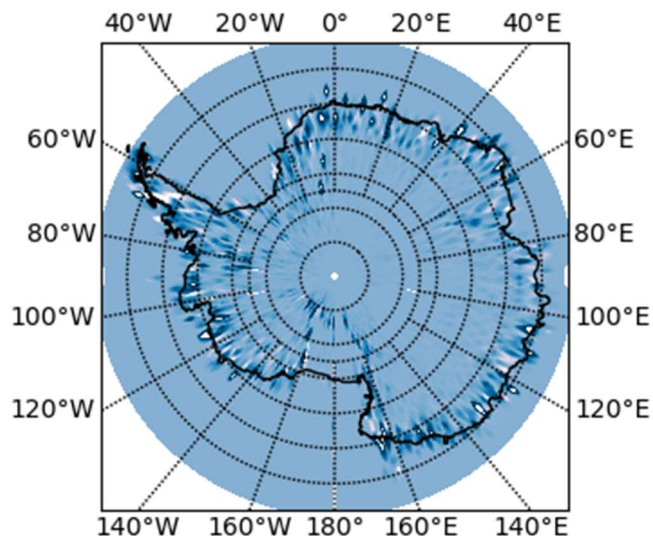


Figure 13 Vernal Equinox 2019 Land-Ice Rates (meters/month)

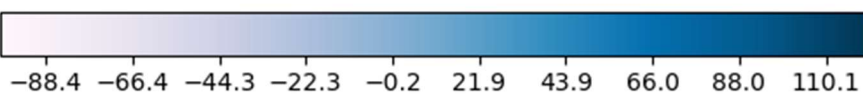
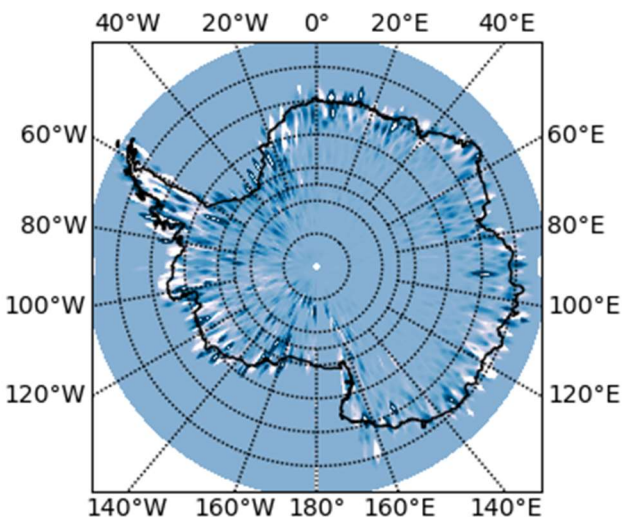


Figure 14 Vernal Equinox 2020 Land-Ice Rates (meters/month)

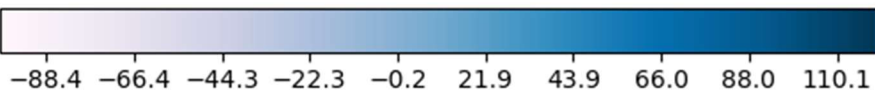
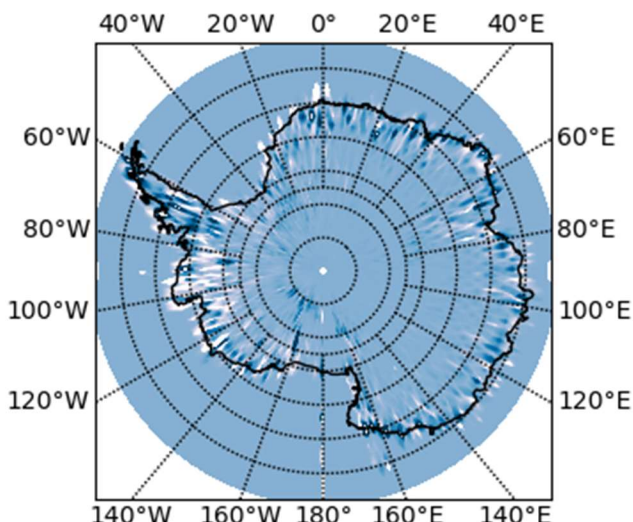


Figure 15 Vernal Equinox 2021 Land-Ice Rates (meters/month)

2. Summer Solstice Land-Ice Change Rates

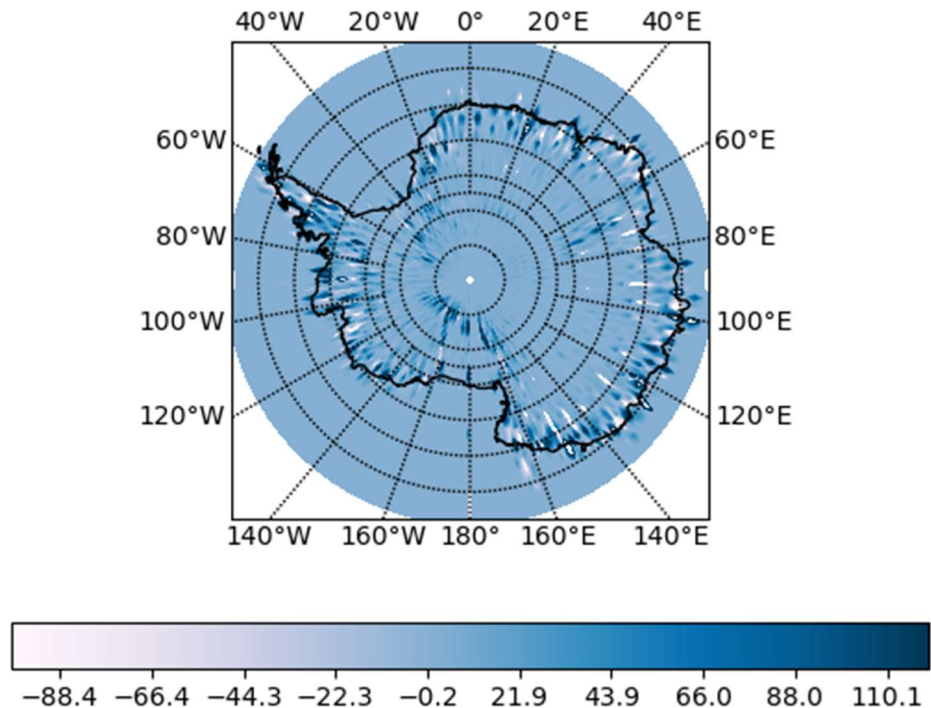


Figure 16 Summer Solstice 2019 Land-Ice Rates (meters/month)

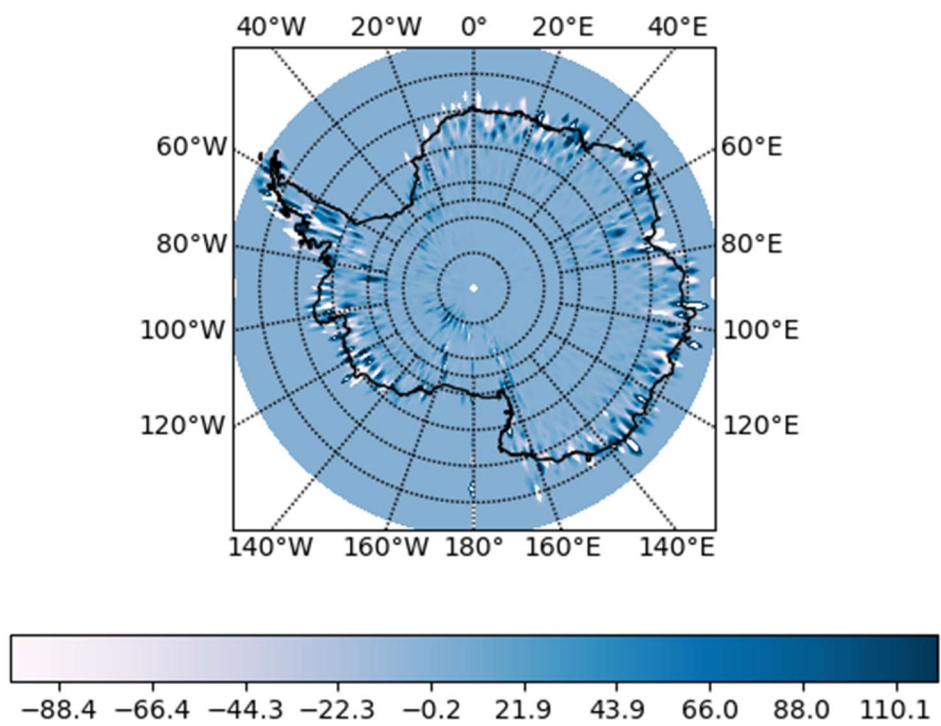


Figure 17 Summer Solstice 2020 Land-Ice Rates (meters/month)

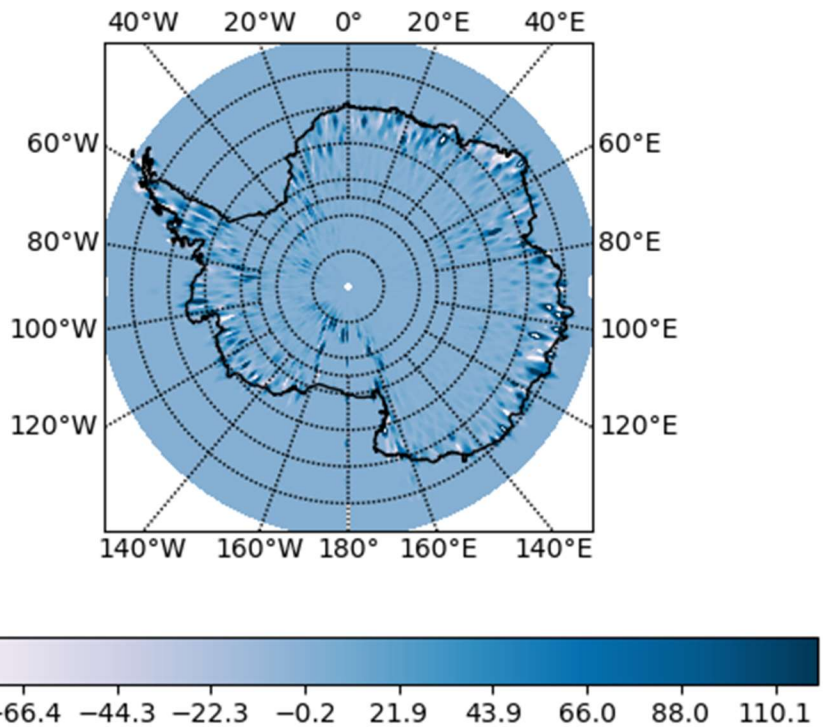


Figure 18 Summer Solstice 2021 Land-Ice Rates (meters/month)

3. Autumnal Equinox Land-Ice Change Rates

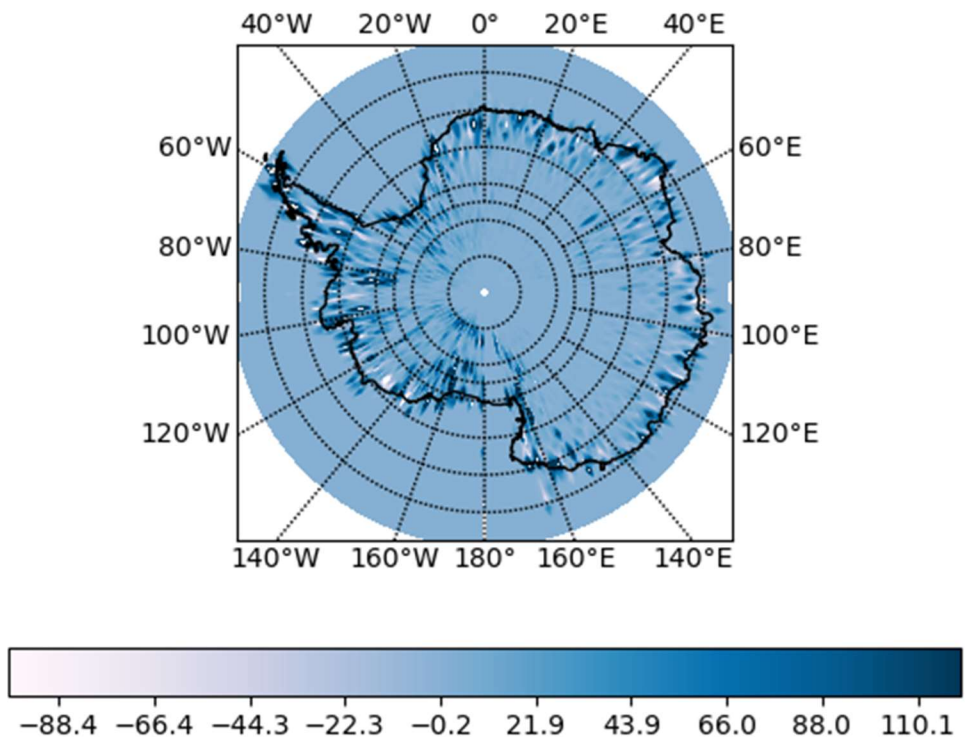


Figure 19 Autumnal Equinox 2019 Land-Ice Rates (meters/month)

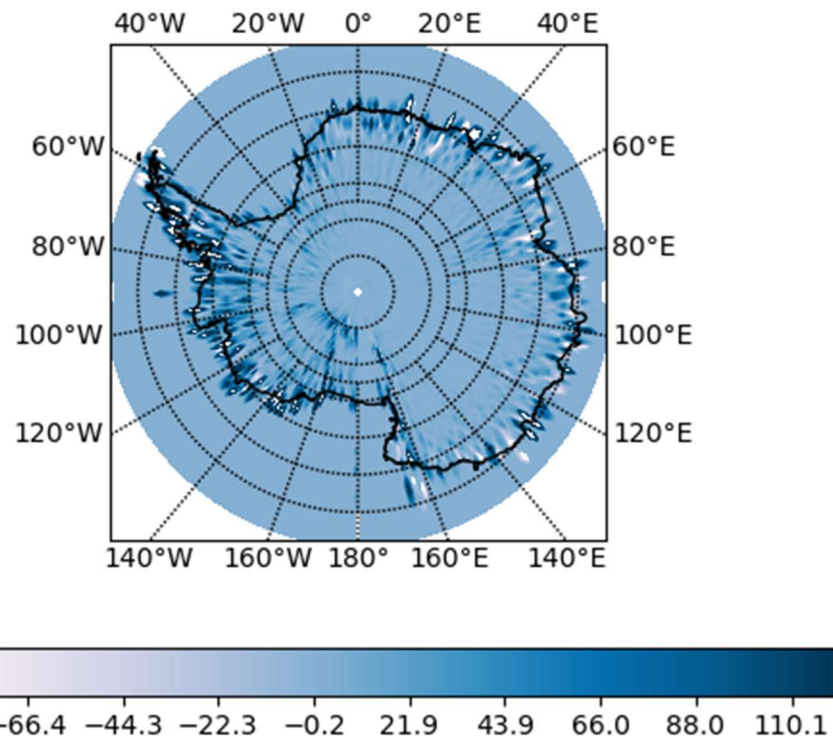


Figure 20 Autumnal Equinox 2020 Land-Ice Rates (meters/month)

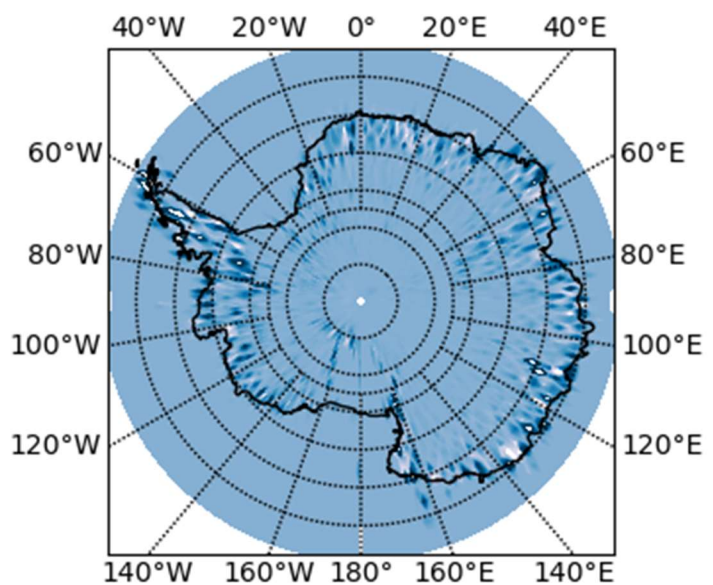


Figure 21 Autumnal Equinox 2021 Land-Ice Rates (meters/month)

4. Winter Solstice Land-ice Change Rates

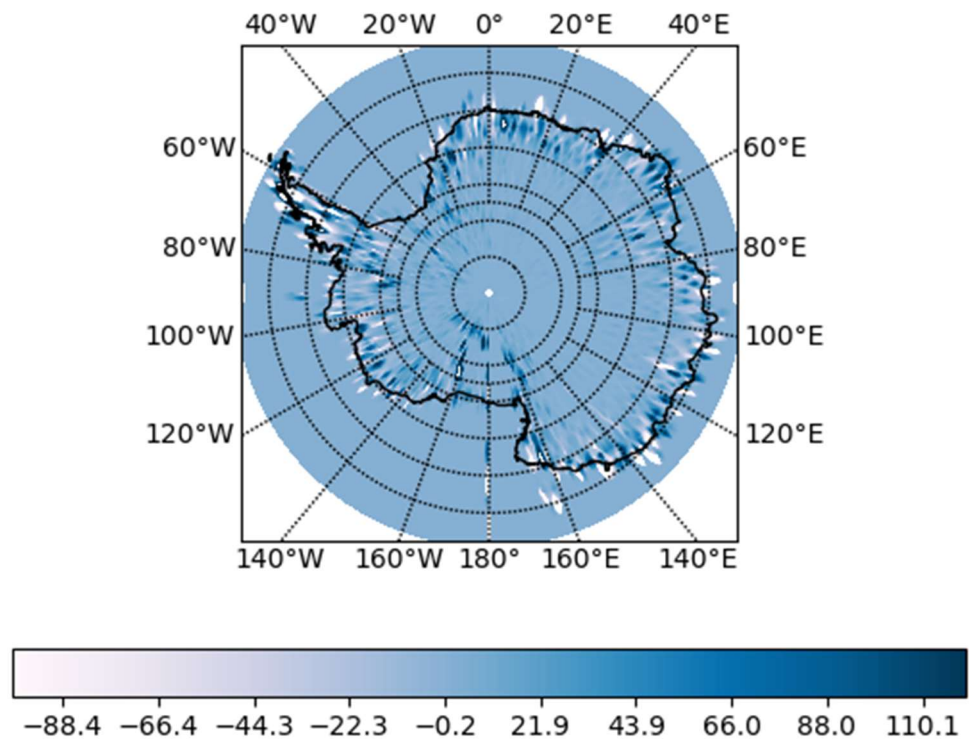


Figure 22 Winter Solstice 2019 Land-Ice Rates (meters/month)

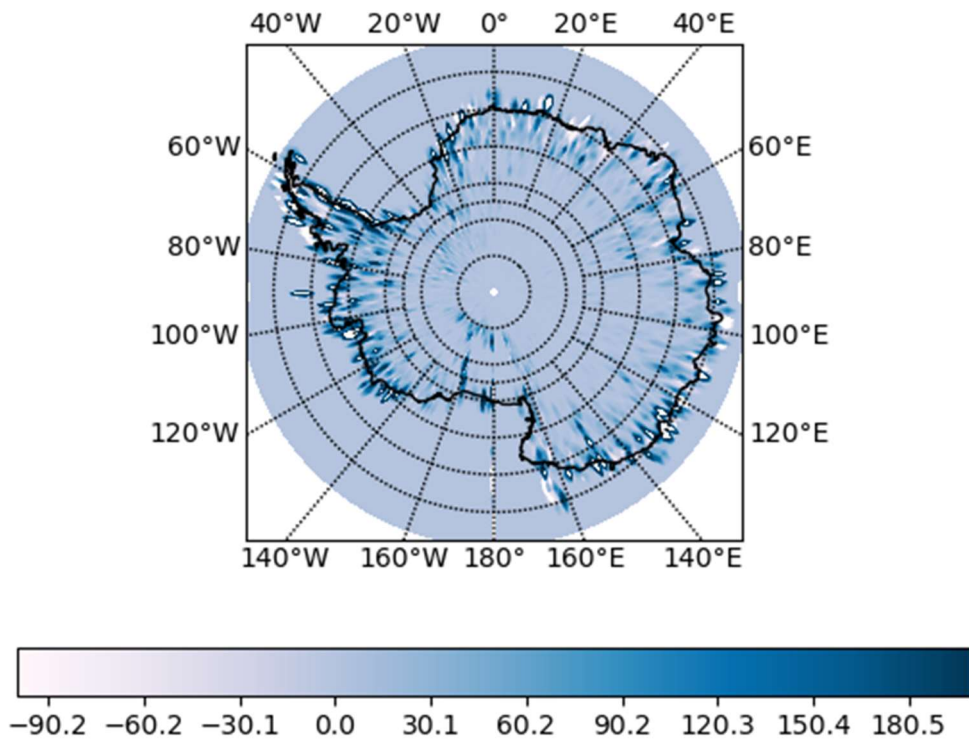


Figure 23 Winter Solstice 2020 Land-Ice Rates (meters/month)

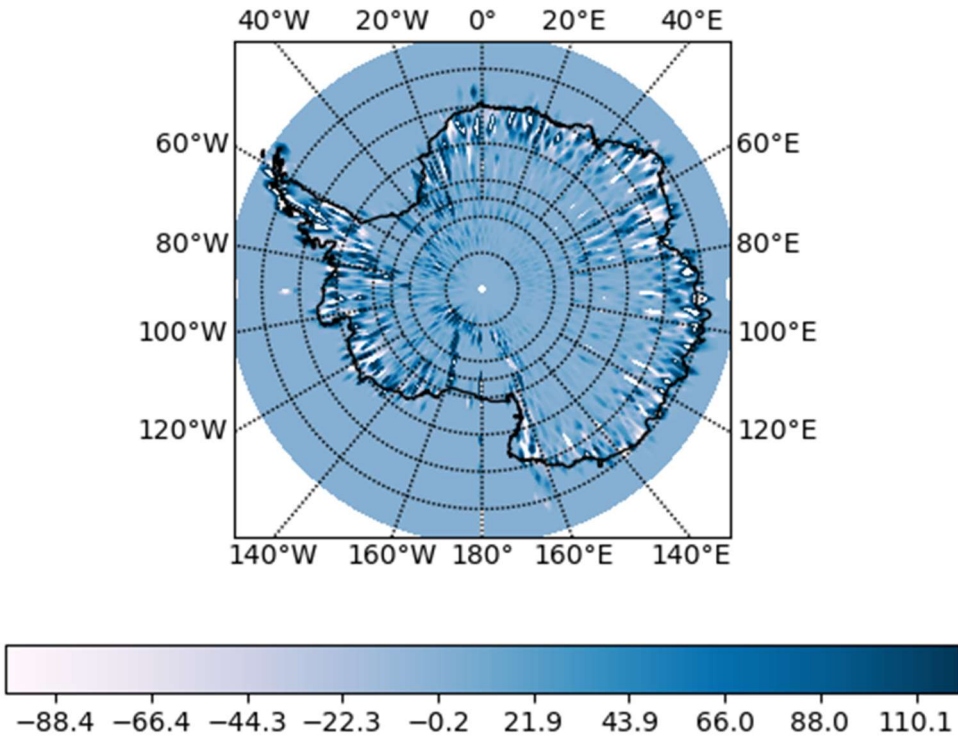


Figure 24 Winter Solstice 2021 Land-Ice Rates (meters/month)

5. Power Spectrum at Locations on the West Coast

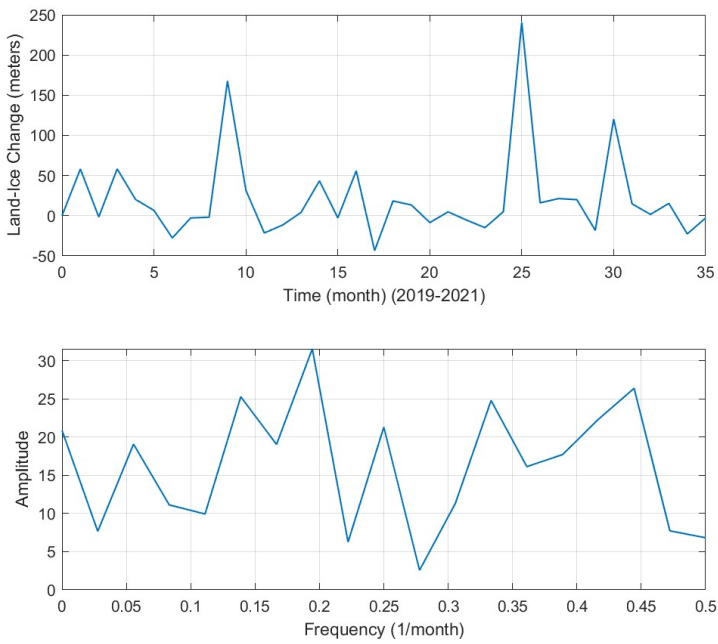


Figure 25 Land-Ice Level Change (Since Jan 2019) Time Series and Power Spectrum at Lon = -104.5 deg Lat = -77.5 deg

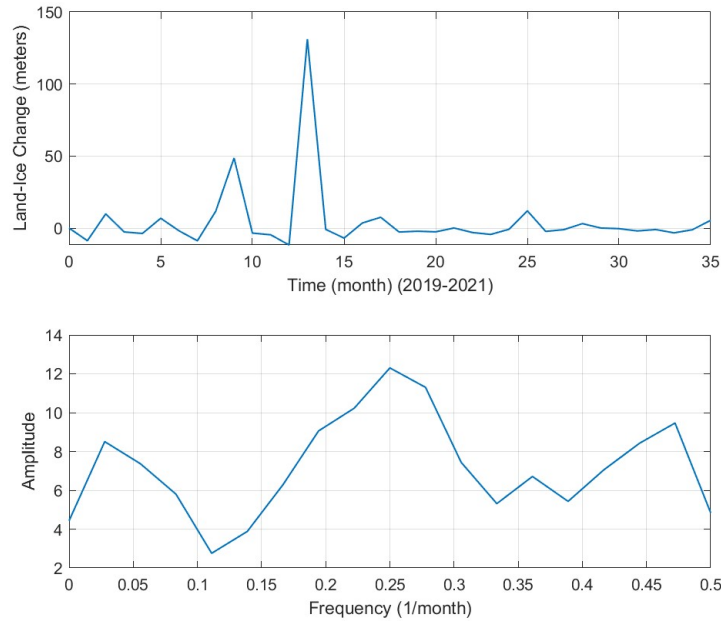


Figure 26 Land-Ice Level Change (Since Jan 2019) Time Series and Power Spectrum at Lon = -104.5 deg Lat = -81.5 deg

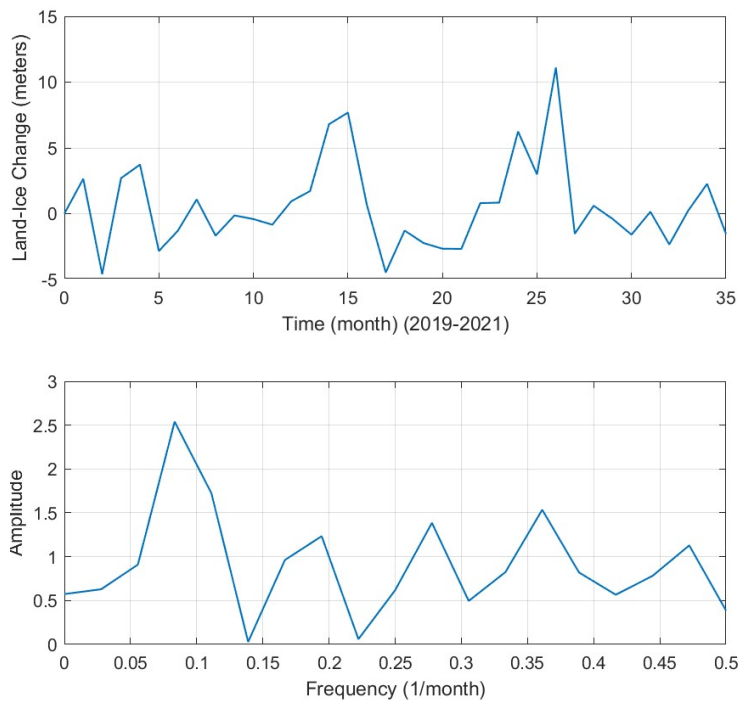


Figure 27 Land-Ice Level Change (Since Jan 2019) Time Series and Power Spectrum at Lon = -104.5 deg Lat = -87.5 deg

6. Icesat-2 EOF Analysis

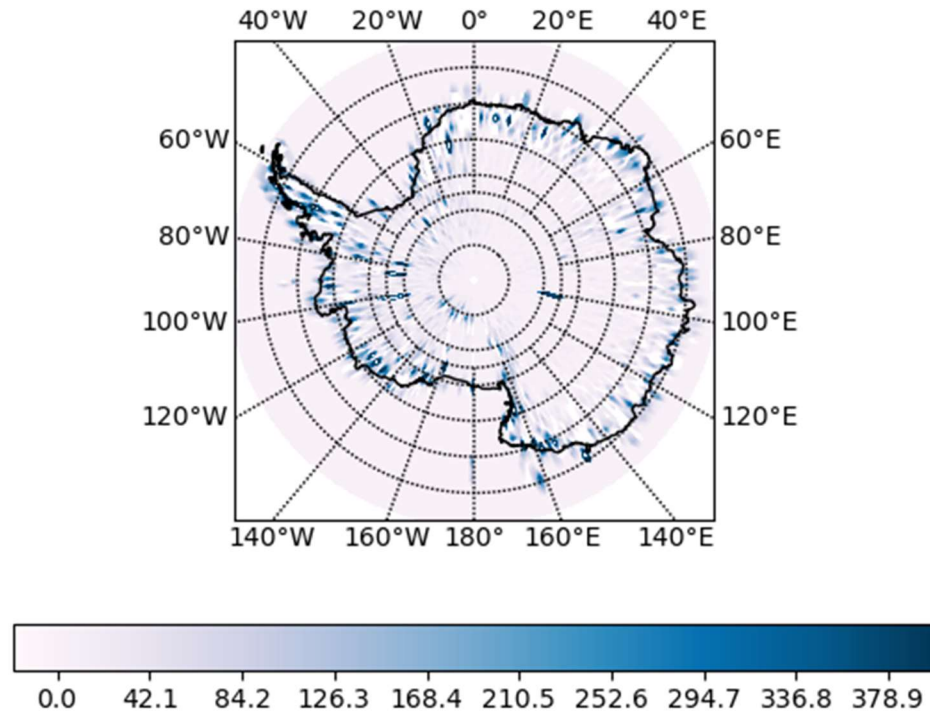


Figure 28 EOF Mode 1 accounting for 62.687% of Variance

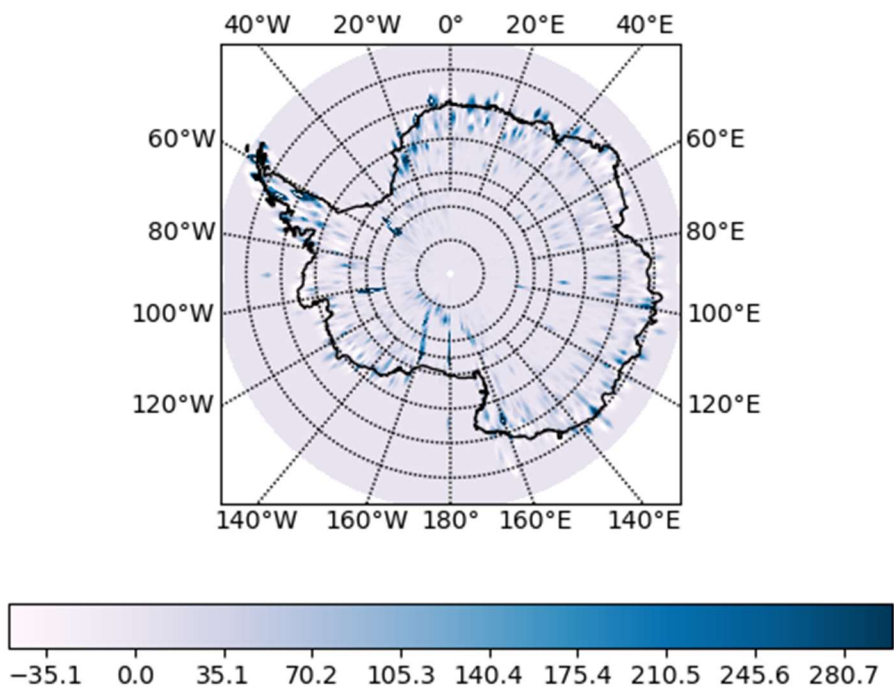


Figure 29 EOF Mode 2 accounting for 27.75% of Variance

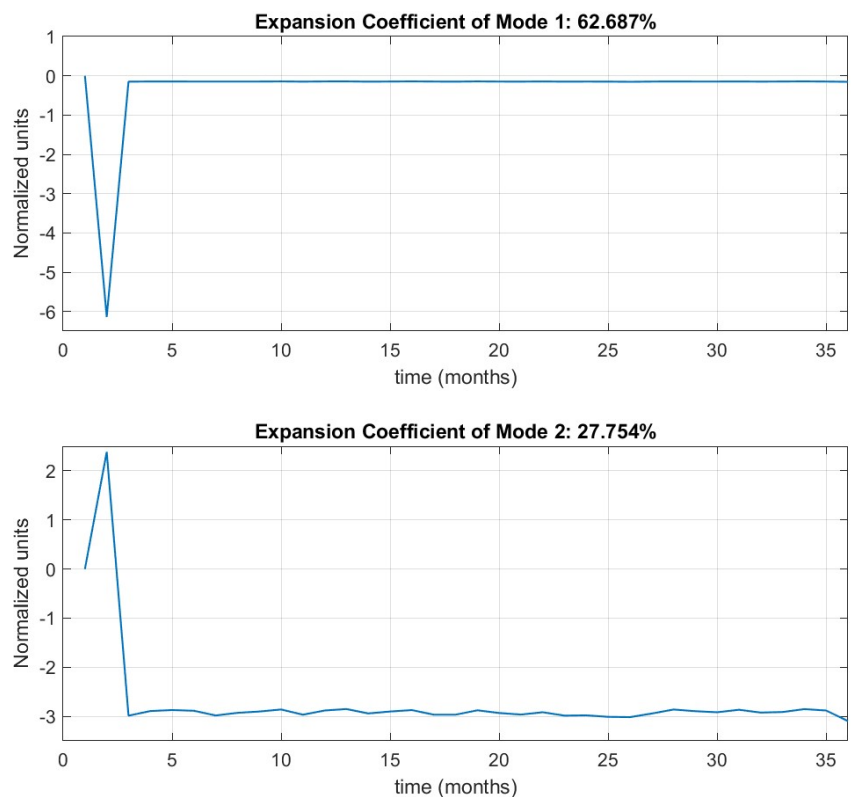


Figure 30 Expansion Coefficients (Time Series) of Modes 1 & 2

7. Icesat-2 and Grace Coupled EOF Analysis

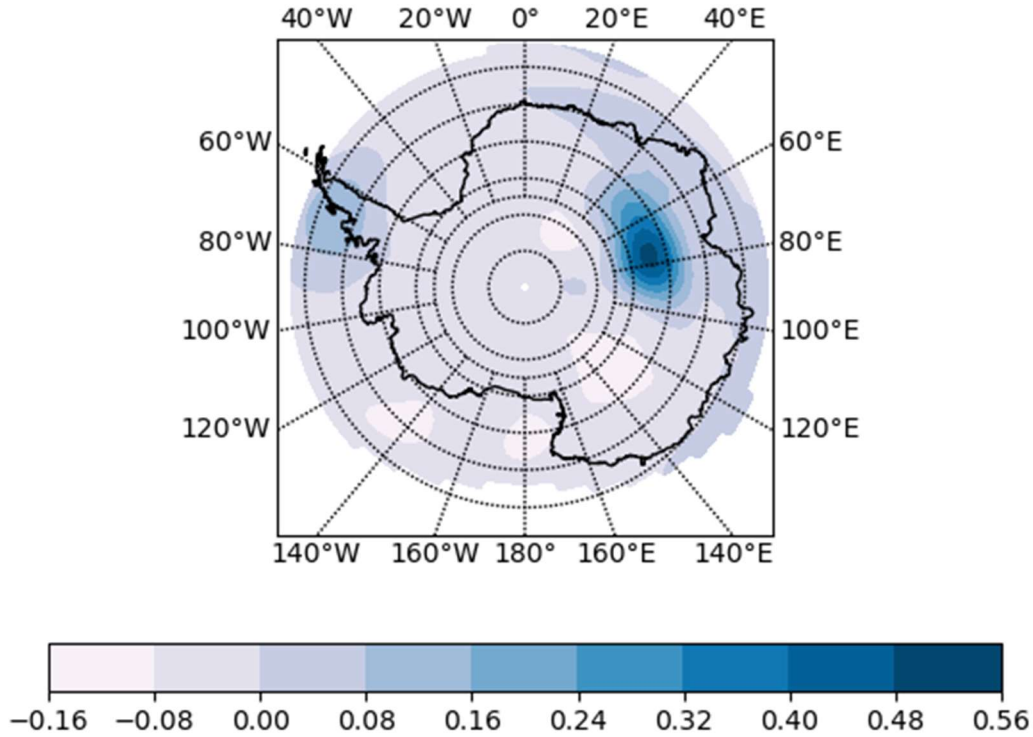


Figure 31 Icesat-2 and Grace EOF Mode 1 (Feb 2019) accounting for 99.957% of Variance

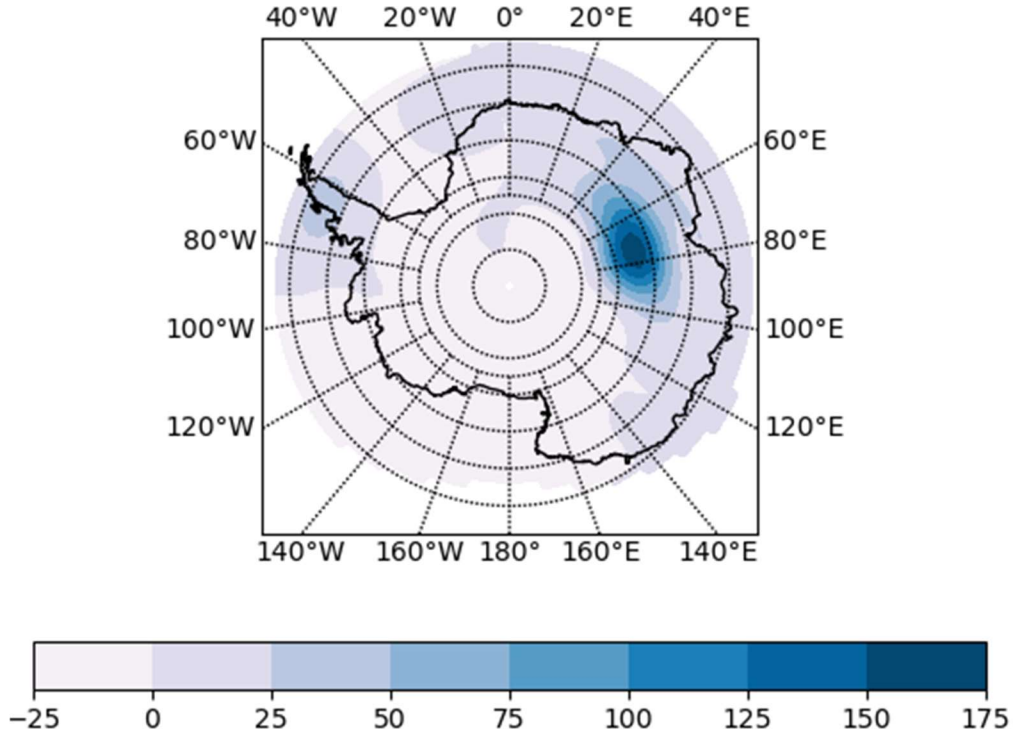


Figure 32 Icesat-2 and Grace EOF Mode 1 (Jan 2020) accounting for 99.957% of Variance

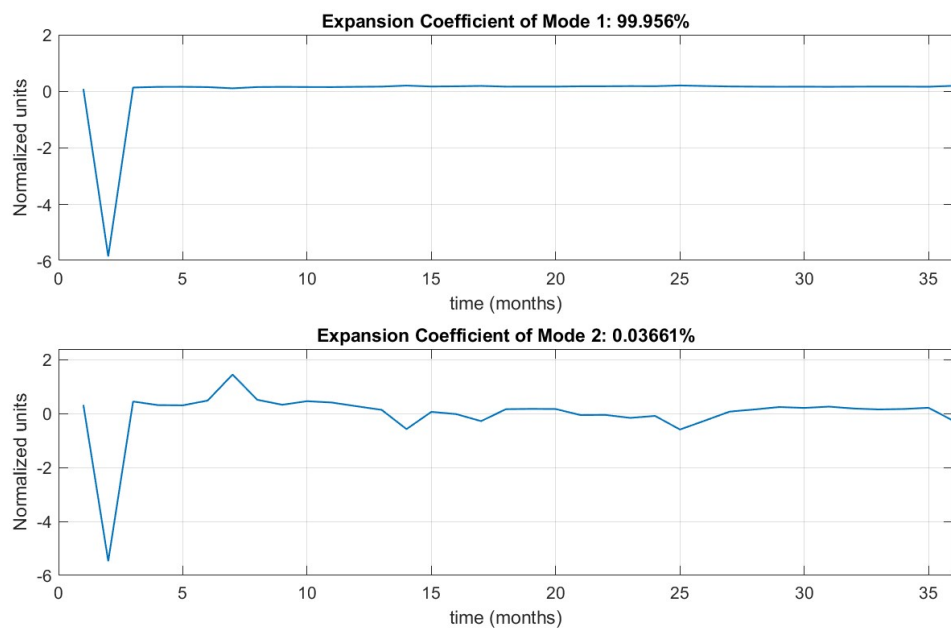


Figure 33 Expansion Coefficients (Time Series) of Icesat Covariance Modes

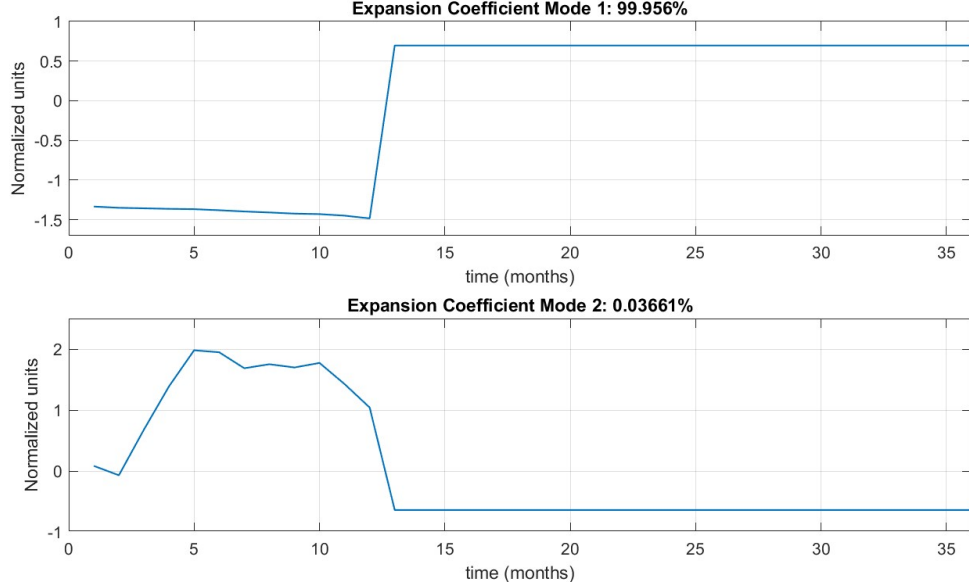


Figure 34 Expansion Coefficients (Time Series) of Grace Covariance Modes

V. Discussion

E. GRACE-FO Analysis

1. Time Series and Spectral Analysis

The time series and periodograms in Figures 3-5 show much of the variability that was anticipated for this more volatile region of West Antarctica. The 87.5° S plot represents a chiefly annual (337 days) frequency component with small peaks for semi-annual (151 days) and multi-annual frequencies. The 81.5° S plot shows similar results, with a larger presence of a multi-annual peak of 1095 days, nearly exactly three years. The equivalent water height of the mass changes in each of these regions is minimal, and little evidence of a trend can be found within these cumulative time series. At a latitude of 77.5° S, this is not quite true. Among maps generated for the cumulative time series, the region of West Antarctica surrounding this point demonstrated the largest trend in ice mass loss. This is made clear in the periodogram, where low frequency trend signals compose the bulk of the signal. Of note is the large spike between January and February of 2019 in the time series. This can possibly be traced to the weakening of the polar vortex, a high-altitude wind pattern, in January 2019. This trend was noticed in other measurements, as a record low for Antarctic sea ice extent was recorded during this month [6]. The magnitude of this change is noticeable in the primary EOF modes as well, as an otherwise unaccounted for high frequency component. For the 77.5° S point as a whole, a general trend was still more present after January of 2019 than in the others observed, with a loss of nearly 1 centimeter over the rest of the time series. Annual and bi-annual components are also apparent.

2. EOF Analysis

Of more interest to the results of the study are the EOF modes determined. The first three modes were calculated to explain 66.91, 14.89, and 5.20 percent of the total variability in the data, respectively. The first EOF mode holds interesting results, the first of which likely corresponds to the January to February 2019 spike mentioned above. The same relatively extreme change is visible in this interval for the first expansion coefficient time series in Figure 6. On the periodogram, a sharp peak occurs at the Nyquist frequency of half the sampling rate of approximately 30 days. With no other noticeable high frequency trends, that event was likely the cause. Figures 9 and 12 show the first two timesteps of the mode geographically. The second time step provides more insight into the general trend, ignoring the initial spike. This mode is primarily tied to the trend-dominated pattern in the volatile West

Antarctic region. Annual periodicity is visible, though the majority of the mode explains the long-period temporal trend with a specific spatial region. Because this mode is responsible for such a high fraction of the total variance, it again demonstrates the relative magnitude of the decrease of ice mass within that particular region. Possible issues introduced by the detrending of data likely had a significant impact on this mode. The detrend was used in order to isolate the annual and sub-annual signals so that the EOF modes would reflect seasonal and other higher frequency trends. The spike in the time series signal likely lowered the correlation of the linear fit for detrending. This means that for the remainder of the time series, where data appeared to be approximately linear, a trend was possibly introduced. It appears that this mode primarily captures that unintended variation.

The second mode, describing nearly fifteen percent of the total variance, is shown by Figure 7. This mode is dominated by an annual signal with a period calculated to be just over 365 days. No trend or other signals are apparent. Geographically, this impacts different regions with slightly varying effects. As shown by the yellow regions in Figure 10, much of central Antarctica has minimal annual change in mass. Small mass decreases can be seen in some Southwestern, Eastern, and Northern regions. Small increases can be seen especially on the Eastern and Western coasts, indicating a general redistribution of mass to the coastal areas.

Describing just over five percent of the variance, the third mode is temporally composed of a semi-annual component of 168 days and a multiannual component of three years, as is visible in Figure 8. Figure 11 demonstrates the spatial impact of these components, which results in a less radially varied output than the second mode. Eastern regions are relatively unaffected, while the lower-elevation Western Antarctic demonstrates various effects. Much of the region shows a decreasing expansion coefficient, while the Antarctic Peninsula shows a more significant decrease.

F. Icesat-2 Analysis

1. Land-Ice Level Rates

It is inherent that from the summer solstice to autumnal equinox there will be an increase land-ice levels since the Antarctic south pole faces away from the sun, and during winter solstice to spring equinox, there will be a decrease in land-ice level since the south pole faces the sun.

During the summer solstice, figures 16-18, a trend of positive land-ice rates has been declining slowly over the years. For the autumnal equinox, the year 2019 showed higher positive ice-level rates especially in the inland areas of the Antarctic west coast which has decreased in 2021.

During the spring equinox, figures 13-15, there is a trend of positive and negative land-ice level rates along the coasts. Over the years 2019-2021, the negative land-ice level rates are growing and are starting to dominate along the west coast indicating a depletion in ice levels. Similarly, during the Winter Solstice, figures 22-24, the negative land-ice rates are starting to dominate over both coasts of Antarctica and the positive rates have declined from nearly 180 meters/month to 110 meters/month.

2. Power Spectrum Analysis

The time series of the ice levels at the key locations, figures 25-27, unexpectedly, do not have a periodic pattern. At latitude 77.5 S, there appears to be peaks, indicating increase in ice-levels, during September 2019 and 2021. At latitude 81.5 S, there is a peak during August 2019, and January 2020. At latitude 87.5 S, the dominant peaks occur on April 2020 and 2021. The power spectrum results at these grid locations are inconclusive since they do not produce periodic increase or decrease in ice levels in the time series. Moreover, the power spectrum is hard to interpret since the sampling frequency of 1 sample per month is too low. Additionally, the patterns in the time series and power spectrum for Icesat and grace at these grid locations does not look comparable, therefore, there is no indication whether changes in ice-levels affect the gravimetry results.

3. Icesat-2 EOF Analysis

From the EOF analysis, EOF 1 accounts for 62.687% of variances in land-ice levels and EOF 2 accounts for 27.75% of the variances in Antarctic land-ice levels. Modes lower than 3 account for ~0.02% of all variances and are unaccounted for. Figure 28 is the reconstructed Land-Ice level contribution due to EOF 1 and figure 29 is for EOF 2. Figure 30 provides the expansion coefficients of the EOFs which provides the trend in of the time series of the EOFs, the coefficients are normalized by the standard deviation. It is evident that there is a negative peak for EOF 1 and positive peak for EOF 2 during February 2019. For the rest of the months, EOF 1 remains stagnant at 0 whereas as EOF 2 remains near constant at -3. The EOFs for the Icesat-2 are not periodic in nature.

4. Icesat-2 & Grace coupled EOF Analysis

The EOF analysis of the coupled Icesat-2 land-ice level and Grace gravimetry covariances will determine the variances in the relationships between the datasets. It was found the EOF1 mode accounted for 99.957% of all variances and EOF mode 2 accounted for 0.03661% of the variances, modes less than 2 accounts for less than ~0.001% of the variances and were ignored. Figures 31 and 32 are the reconstructed EOF 1 modes for the month of Feb 2019 and January 2020. The contour plots show high covariance bounded by latitudes 40°E and 100°E. Additionally, the Grace data points at some locations were unequally spaced due to coasts, therefore, linear interpolation was used to remap the data points into equally spaced grids for plotting.

Figures 33 and 34 provides the time series of the 2 modes for the case of Icesat and Grace normalized by the standard deviation. For mode 1 of 99.957% variance for Icesat-2 has similar plot to that of figure 30 with a negative peak during the month of Feb 2019. For mode 1 for the case of Grace, there EC remains constant at nearly -1.5 which switches to 0.69 between Jan to Feb 2020 and remains constant from there. Unlike the Grace EOF results, the EOFs are not periodic in nature for the case of the coupled fields.

5. Limitations and Further improvements

The time series and power spectrum analysis were limited by the sampling rate, in this case, 1 month was taken since Icesat-2 needed to orbit sufficient number of time to record data that covered the whole of antarctica. Additionally, as the Satellite passes from south to north, the data points collected become more sparse, and sometimes, there are very few grid points that are sampled at higher latitudes since the longitudes diverge. Sampling more satellite tracks could solve this issue but might increase the sampling frequency.

For averaging, the data points were simply sorted into grid centers since the number of data points were far too large to be processed. This could cause an issue since the averaged data points could be around a different coordinate within the grid cell. Also, as we move towards the south pole, the grid sizes contain smaller area and would not properly represent the average. A better way would be to average points within a given distance radius of the grid points since this will be able to capture averages properly.

VI. Conclusion

Independent analysis of the GRACE-FO data over the period of 2019 to 2021 revealed a handful of dominant patterns. The three primary modes of the EOF study described over 87% of the total variation of the data. The first mode, although possibly interfered with by detrending, highlighted the strong linear trend in the West Antarctic region, as well as a small annual signal in other regions. The second mode clearly showed the annual frequency of mass variation and suggested a pattern of redistribution of mass from central regions to coastal ones. The final mode studied combined a three-year signal and a semi-annual signal, demonstrating mass losses and accumulation in different sections of Western Antarctica.

From 2019 to 2021, negative land-ice level rates of nearly -90 meters/month are starting to dominate during the winter solstice and spring equinox, and during the summer solstice and autumnal equinox, positive rates have declined from nearly 180 meter/month to 110 meters per month at several locations around the coasts, particularly on the west side. For the case of time series and power spectrum at key locations, there are peak ice change once or twice between

2019 and 2021 and do not have a periodic change, and the power spectrum was inconclusive since sampling frequency was lower than Nyquist frequency. Moreover, the patterns are incomparable to Grace results. The EOF results indicated a 62.687% variance for EOF1, a 27.75% variance for the second EOF. The coupled Icesat-2 and Grace field covariance results indicates a 99.957% variance in mode 1, having high covariance on the East coast.

References

- [1] Kwok, R., G. Cunningham, T. Markus, D. Hancock, J. H. Morison, S. P. Palm, S. L. Farrell, A. Ivanoff, J. Wimert, and the ICESat-2 Science Team. 2019. *ATLAS/ICESat-2 L3A Sea Ice Height, Version 2*. [Indicate subset used]. Boulder, Colorado USA. NSIDC: National Snow and Ice Data Center. doi: <https://doi.org/10.5067/ATLAS/ATL07.002>. [Date Accessed].
- [2] Landerer, F., “CSR TELLUS GRACE Level-3 Monthly Land Water-Equivalent-Thickness Surface Mass Anomaly Release 6.0v04,” Jun. 2021.
- [3] Landerer, F., and Cooley, S., Pasadena, CA: NASA JPL, “GRACE-FO Level-3 Data Product User Handbook,” May 2021
- [4] Zechmeister, M., and Kürster, M., “The generalised Lomb-Scargle Periodogram,” *Astronomy & Astrophysics*, vol. 496, 2009, pp. 577–584.
- [5] Shea, D., “The Climate Data Guide: Empirical Orthogonal Function (EOF) Analysis and Rotated EOF Analysis,” *NCAR - Climate Data Guide* Available: <https://climatedataguide.ucar.edu/climate-data-tools-and-analysis/empirical-orthogonal-function-eof-analysis-and-rotated-eof-analysis>.
- [6] Bjornsson, H., and Venegas, S. A., “A Manual for EOF and SVD Analyses of Climatic Data,” *CCGCR Report*, vol. 97, 1997, pp. 112–134.
- [7] “Polar Vortex Breakdown,” *NSIDC Arctic News and Analysis RSS* Available: <http://nsidc.org/arcticseaincnews/2019/02/>.
- [8] Scheick, J. *et al.*, (2019). icepyx: Python tools for obtaining and working with ICESat-2 data. <https://github.com/icesat2py/icepyx>.